Available online at www.sciencedirect.com
SCIENCE DIRECT®
Journal of Solid State Chemistry 178 (2005) 1230–1240
JOURNAL OF SOLID STATE CHEMISTRY
www.elsevier.com/locate/jssc

$LiMO_2$ (M = Mn, Fe, and Co): Energetics, polymorphism and phase transformation

Miaojun Wang, Alexandra Navrotsky*

Thermochemistry Facility and NEAT ORU, University of California at Davis, One Shields Avenue, Davis, CA 95616, USA

Received 17 December 2004; received in revised form 27 January 2005; accepted 28 January 2005

Abstract

$LiMO_2$ materials (M = Mn, Fe, and Co) with different structures were synthesized and their enthalpies of formation from oxides (Li_2O and M_2O_3, M = Mn and Fe), or from oxides (Li_2O and CoO) plus oxygen at 25 °C were determined by high-temperature oxide melt solution calorimetry. The relative stability of the polymorphs of the compound $LiMO_2$ was established based on their enthalpies of formation. Phase transformations in $LiFeO_2$ were investigated by differential scanning calorimetry and high-temperature oxide melt solution calorimetry. The phase transition enthalpies at 25 °C for $\beta \rightarrow \alpha$, $\gamma \rightarrow \beta$, and $\gamma \rightarrow \alpha$ are 4.9 ± 0.7, 4.3 ± 0.8 and 9.2 ± 0.9 kJ/mol, respectively. Thus the γ phase (ordered cations) is the stable form of $LiFeO_2$ at room temperature, the α phase (disordered cations) is stable at high temperature and the β phase may have a stability field at intermediate temperatures.

Keywords: $LiMO_2$; Battery materials; Enthalpy of formation; Phase transformation; Rock-salt

1. Introduction

Ternary lithium first row transition metal oxides $LiMO_2$ exhibit a variety of crystal structures, most of which are derivatives of the rock-salt structure [1]. The different structures result from different cation arrangements within the cubic close packed array of oxygen ions. These structures can be classified into five categories (Table 1) [1–3].

With soft chemistry synthesis or electrochemical methods, many compounds can be prepared with structures other than that of the thermodynamically stable phase. Metastable $LiMnO_2$, $LiFeO_2$ with the α-$NaFeO_2$ structure can be synthesized through soft chemistry routes such as ion exchange [4–6]. The Jahn–Teller effect of Mn^{3+} ions reduces the symmetry of the structure to monoclinic. $LiFeO_2$ isostructural with $LiMnO_2$ was synthesized by Kanno et al. by H^+/Li^+ ion exchange from γ-FeOOH [7]. $Li_2Ti_2O_4$ (from lithiation of $LiTi_2O_4$ spinel), $Li_2Mn_2O_4$ (from lithiation of $LiMn_2O_4$ spinel), $LiVO_2$ synthesized at high pressure and $LiCoO_2$ synthesized at low-temperature (LT-$LiCoO_2$) crystallize in the atacamite-type structure. $LiCoO_2$ has a different layered structure which is denoted as O2 type according to the packing designation proposed by Delmas et al. [8]. The letter P, T or O describes the coordination geometry of A site ions (prismatic, tetrahedral or octahedral, respectively), and the number 1, 2 or 3 indicates the number of MO_2 slabs within the unit cell. In this notation, the layered α-$NaFeO_2$ structure is of O3 type.

Many of these compounds are of interest for lithium battery applications. The layered structure is ideal for lithium intercalation/deintercalation. The structural stability of $LiMO_2$ was investigated by Wu et al. [9] using theoretical calculations. Their calculations showed that the size difference between the transition metal ion and the lithium ion (or the ratio of $r_{M^{3+}}/r_{Li^+}$) affects the stability of the $LiMO_2$ structures. The α-$NaFeO_2$ structure is stabilized for M cations with a radius much different from that of the Li ion [9]. $LiMnO_2$ is an

*Corresponding author. Fax: +530 752 9307.
E-mail address: anavrotsky@ucdavis.edu (A. Navrotsky).

0022-4596/$ - see front matter © 2005 Elsevier Inc. All rights reserved.
doi:10.1016/j.jssc.2005.01.028

Table 1
Structures of LiMO_2 compounds

	Structure	Description	Space Group	Compounds
(1)	α-$NaFeO_2$ structure	Lithium ions and transition metal ions are ordered in alternating (111) planes	$R\bar{3}m$	LiMO_2 (M = V, Cr, Co, Ni)
(2)	α-$LiFeO_2$ structure	Lithium ions and the transition metal ions distributed randomly on the octahedral sites	$Fm3m$	α-$LiFeO_2$ $LiTiO_2$
(3)	$LiMnO_2$ structure	An orthorhombic superstructure with alternating zigzag layers of lithium and transition metal ions	$Pmnm$	$LiMnO_2$
(4)	γ-$LiFeO_2$ structure	A tetragonal superstructure with lithium and transition metal ions completely ordered on the octahedral sites	$I4_1/amd$	$LiScO_2$ γ-$LiFeO_2$
(5)	Atacamite-type superstructure	In this spinel-related structure, lithium and transition metal ions occupy 16c and 16d sites, respectively	$Fd3m$	$Li_2Ti_2O_4$ $Li_2Mn_2O_4$ LT-$LiCoO_2$ HP-$LiVO_2$

exception to this rule due to the large magnetic moment and Jahn–Teller effect of high spin Mn^{3+} ions. These two features apparently make the orthorhombic structure more stable than the monoclinic layered structure [10].

In this study, different polymorphs of LiMO_2 (M = Mn, Fe, and Co) were synthesized. Their enthalpies of formation were determined using high-temperature oxide melt solution calorimetry. The relative stability of the polymorphs is investigated.

$LiFeO_2$ provides a good example for studying cation ordering in the rock-salt structure. α-$LiFeO_2$ has a disordered rock-salt structure. Cation ordering starts to occur on annealing at 320 °C and at 530 °C the completely ordered γ phase is formed, which in turn transforms to the α phase at 660 °C [11,12]. The phase transition from α to γ is through an intermediate β phase and the structure of this phase was reported to be tetragonal [11,12] or monoclinic [13]. There are additional tetragonal β phases with different c/a ratios denoted as β′ and β″ [3]. However, direct experimental determination of the phase transformation enthalpy has not been reported and it is not clear which of the phases are metastable and which transitions irreversible. In this work, we studied the phase transformations in $LiFeO_2$ by differential scanning calorimetry (DSC) and determined the enthalpies of the phase transitions using high-temperature oxide melt solution calorimetry. The stability of the three phases (α, β, and γ) at room temperature and at high temperature, is discussed.

2. Experimental

2.1. Sample synthesis

α-$LiFeO_2$ was synthesized from the solid-state reaction of Li_2CO_3 and α-Fe_2O_3. The starting materials were well mixed with an alumina mortar and pestle, pelletized, and calcined at 800 °C in air for 24 h with an intermediate grinding. The product was quenched from 800 °C into ice. β-$LiFeO_2$ was obtained by annealing the above-obtained α-$LiFeO_2$ at 400 °C in air for 16 and 24 days. γ-$LiFeO_2$ was prepared by annealing α-$LiFeO_2$ at 475 °C in air for 12 and 30 days. α-$NaFeO_2$ structured $LiFeO_2$ were synthesized from ion exchange of α-$NaFeO_2$ in molten LiCl–KCl eutectic melt at 380 °C for 3 h followed by washing with hot deionized water and cold deionized water and then dried under vacuum at room temperature [6]. The precursor α-$NaFeO_2$ was prepared from solid-state reaction of γ-Fe_2O_3 and Na_2O_2. The stoichiometric amount of starting materials were weighed and mixed in an argon-filled glove box (oxygen and water level <1 ppm) and calcined at 500 °C for 36 h with an intermediate grinding in the glove box.

O2-$LiCoO_2$ was synthesized from ion exchange of $Na_{2/3}CoO_2$ in a 5 M aqueous solution of LiCl and LiOH (1:1) at 100 °C (water bath) for 24 h with refluxing [14]. The sample was washed with deionized water and dried at 100 °C under vacuum. $Na_{2/3}CoO_2$ precursor was prepared from the solid-state reaction of Na_2CO_3 and Co_3O_4. The stoichiometric mixture was heated at 800 °C in air for 24 h and quenched in air. The product was transferred to an argon-filled glove box when still hot and ground in the glove box. The powders were wrapped in platinum foil and then heated at 800 °C in flowing oxygen for 24 h and quenched into liquid nitrogen.

Monoclinic $LiMnO_2$ (m-$LiMnO_2$) was prepared from ion exchange of α-$NaMnO_2$ in a 4 M n-hexanol solution of LiBr with 6 times the stoichiometric amount of LiBr at 145–154 °C for 24 h with stirring and refluxing [5]. m-$LiMnO_2$ was obtained by washing the product first with n-hexanol and then methanol and was dried under vacuum at room temperature. α-$NaMnO_2$ precursor was

synthesized from Na_2CO_3 and $MnCO_3$ at 725 °C in air for 48 h with an intermediate grinding in the glove box. The product was quenched from 725 °C and transferred into the glove box. Orthorhombic $LiMnO_2$ (*o*-$LiMnO_2$) was prepared from reacting stoichiometric amount of *β*-MnO_2 and Li_2CO_3. The powders were mixed in an alumina mortar and pestle, pelletized, and calcined at 600 °C in argon for 3 h and then at 800 °C in argon for 6 days with two intermediate grindings. $Li_2Mn_2O_4$ was obtained from chemical lithiation of $LiMn_2O_4$ in a 4 M acetonitrile solution of LiI at 82 °C [15]. The reaction flask with refluxing was put in a water bath maintained at 82 °C. The amount of LiI used was more than 6 times the stoichiometric amount. After refluxing for 12 h, the powders were filtered, washed with acetonitrile and dried at 80 °C.

The α-$NaFeO_2$ structured (O3) $LiCoO_2$ sample is the same as used in Ref. [16].

2.2. Sample characterization

Phase identification and phase purity evaluation were carried out by powder X-ray diffraction on a Scintag PAD V diffractometer using Cu*K*α radiation. FTIR spectroscopy was employed as a complementary technique to check if there was a small amount of carbonate impurity that could not be identified by XRD for the samples synthesized from solid-state reaction involving carbonates and to check if there were any adsorbed organic solvents on *m*-$LiMnO_2$ and $Li_2Mn_2O_4$. The infrared spectra of the solid samples were collected on a Bruker EQUINOX 55 spectrometer in the frequency range of 400–4000 cm^{-1} with a spectral resolution of 4 cm^{-1} using the KBr pellet technique.

Quantitative analysis of the amount of Li_2CO_3 impurity was performed using solid state FTIR. Powdered sample of 1 mg was mixed with 150 mg KBr powders and pressed into a pellet of 13 mm diameter under 300 bar for 1 min. A calibration curve (integral area of the spectral region 1310–1591 cm^{-1} as a function of Li_2CO_3 concentration) was established from three standard samples prepared with known Li_2CO_3 concentrations (~2, 5, and 7 wt% of Li_2CO_3). Mixtures of Li_2CO_3 and MnO_2 were used as the standards. Four spectra for each sample were collected to get an average of the integral area.

For samples synthesized from ion exchange and chemical lithiation, chemical compositions were determined by inductively coupled plasma optical emission spectroscopy (ICP-OES). Water contents of the samples were determined by thermogravimetric analysis (TGA) using a Netzsch STA 449C TGA/DSC analyzer. TGA experiments were carried out in argon (40 ml/min) for $LiMnO_2$ and $LiCoO_2$ and in oxygen (40 ml/min) for $LiFeO_2$.

Weight change experiments were conducted to test the stoichiometry of $LiFeO_2$. The experiment was done on α-$LiFeO_2$ only since both *β*- and *γ*-$LiFeO_2$ were obtained by annealing α-$LiFeO_2$. The weight change in the dissolution of $LiFeO_2$ in molten sodium molybdate ($3Na_2O \cdot 4MoO_3$) contained in a platinum crucible was determined. The crucible with the solvent was heated at 700 °C in air in a muffle furnace several times to achieve constant weight. α-$LiFeO_2$ powders 30–50 mg were then added and dissolved in the solvent by heating at 700 °C. The total weight before and after dissolution was measured using a Mettler Toledo semimicrobalance (Model AT261, 0.01 mg). The weight change is zero within experimental error. This indicates that all iron is trivalent in the $LiFeO_2$ samples, since the oxidation state is Fe^{3+} when iron oxides are dissolved in molten sodium molybdate at 700 °C in air [17,18].

2.3. Thermal analysis

DSC experiments were performed on α-, *β*-, and *γ*-$LiFeO_2$ using a Netzsch STA 449C TGA/DSC analyzer in an oxygen flow of 40 ml/min. About 30 mg samples were heated to 800 °C and cooled to 30 °C. Heating/cooling rates of 10 and 5 °C/min were used. The DSC experiments were performed a second time with the same parameters (denoted second run in the discussion hereafter) on the cooled product. A low cooling rate of 1 °C/min was also tried on *γ*-$LiFeO_2$ which had been heated to 800 °C at 5 °C/min. Then a second DSC measurement at 5 °C/min was done on the cooled product. Phase transition temperatures were determined as the temperatures of the peaks of the DSC traces. Determination of phase transformation enthalpies was not attempted from the DSC data because of the likely incompleteness of the transitions. The enthalpies of phase transitions were determined by high-temperature oxide melt solution calorimetry as described below.

2.4. High-temperature oxide melt solution calorimetry

High-temperature oxide melt solution calorimetry was performed using a custom built Tian–Calvet twin calorimeter described by Navrotsky [19,20] to determine the enthalpy of formation from binary oxides. Samples in the form of pellets (~5 mg) were dropped from room temperature (25 °C) into molten sodium molybdate ($3Na_2O \cdot 4MoO_3$) solvent at 701 °C in platinum crucibles located in the calorimeter chambers. The heat of drop solution (ΔH_{ds}) is the sum of heat content of the sample from 25 to 701 °C and the heat of dissolution into the solvent (with evolution of O_2). The calorimeter is calibrated against the heat content of ~5 mg pellets of high purity α-Al_2O_3 (99.997%). Appropriate thermodynamic cycles were used to determine the enthalpies of formation from binary oxides (and oxygen) at 25 °C for

the complex oxides. Flushing gas over the melt was employed to maintain the desirable atmosphere and bubbling gas introduced into the solvent to stir the melt to prevent local saturation of the solvent. This helps the samples dissolve faster. Oxygen was used as flushing and bubbling gas for the drop solution calorimetry of $LiFeO_2$ and argon for the calorimetric experiments of $LiMnO_2$ and $LiCoO_2$. The final state of cobalt is divalent in sodium molybdate at 701–703 °C in an argon atmosphere [16,21]. The final state of iron is trivalent in oxygen or air [17,18]. The final state of manganese is a mixture of oxidation states but reproducible and constant in a given atmosphere [22].

3. Results and discussion

3.1. Sample characterization

The XRD patterns of the samples are shown in Fig. 1. γ-$LiFeO_2$ samples obtained by annealing α-$LiFeO_2$ at 475 °C for 12 and 30 days are identical by XRD. The XRD patterns of β-$LiFeO_2$ annealed for 16 and 24 days are identical and match that reported by Anderson and Schieber [11]. All samples except $Li_2Mn_2O_4$ are single phase by XRD. There is a small amount of unreacted $LiMn_2O_4$ (<5 wt%) present in $Li_2Mn_2O_4$ (see inset of Fig. 1 (a)). A long scan (dwell time of 10 s) revealed small reflections from Li_2CO_3 in $Li_2Mn_2O_4$ as well.

FTIR is very sensitive to lithium carbonate which is not a good X-ray scatterer. Li_2CO_3 shows vibrational bands at 1440–1500 cm^{-1} and ~870 cm^{-1}. FTIR revealed that there was Li_2CO_3 impurity in the *m*-$LiMnO_2$ sample that was not detected by XRD. The amount of Li_2CO_3 was estimated by quantitative FTIR. The calibration curve (integral area of the spectral region 1310–1591 cm^{-1} vs. wt% of Li_2CO_3) is shown in Fig. 2. The amount of Li_2CO_3 in $Li_2Mn_2O_4$ and *m*-$LiMnO_2$ was estimated to be 3.9 and 6.5 wt%, respectively. For all other samples, no Li_2CO_3 was detected by FTIR (detection limit 0.5 wt% at the experimental conditions). However, the accuracy of the quantitative FTIR analysis depends on the spectra. For the calibration curve method to work, the vibrational band chosen for integration and evaluation should be well resolved and similar in shape for the standard samples and the samples for analyses. The second criterion was not strictly satisfied for $Li_2Mn_2O_4$ and *m*-$LiMnO_2$ and the amounts of Li_2CO_3 determined are probably not very accurate. Thermogravimetric analysis was used to further check the amount of Li_2CO_3.

TGA showed 2.44% and 3.60% weight loss (average of two experiments) in $Li_2Mn_2O_4$ and *m*-$LiMnO_2$, respectively. This weight loss was ascribed to the decomposition of Li_2CO_3. Thus the amount of Li_2CO_3 impurity was calculated to be 4.1 and 6.0 wt% in

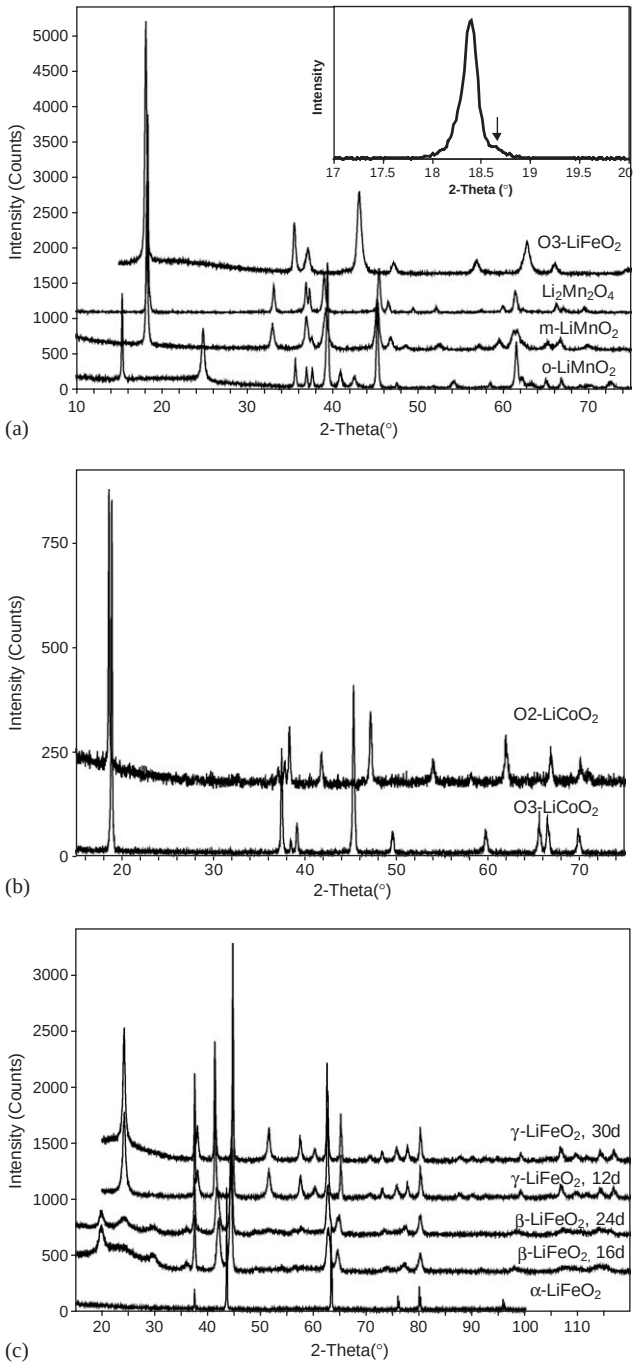

Fig. 1. XRD patterns of Li*M*O_2. The hump at low angles is from the glass sample holder. Arrow indicates $LiMn_2O_4$ impurity.

$Li_2Mn_2O_4$ and *m*-$LiMnO_2$ and was used to correct the enthalpy of drop solution.

No weight change occurred during TG heating/cooling for α-, β-, or γ-$LiFeO_2$. This indicates that there is no adsorbed water on these samples. O2-$LiCoO_2$ has a weight loss of ~0.2%, presumably from surface water. No calorimetric correction was done for this small amount of water because such a correction would be

within experimental error. O3-$LiFeO_2$ showed a weight loss of 0.58% (average of two measurements) and correction of the enthalpy of drop solution was made assuming physisorbed water (adsorption enthalpy equal to condensation enthalpy of water, i.e., 44.0 ± 0.1 kJ/mol at 25 °C [23]).

The results of ICP analyses for *m*-$LiMnO_2$, O2-$LiCoO_2$, O3-$LiFeO_2$ and $Li_2Mn_2O_4$ are listed in Table 2. These chemical compositions were used in calorimetric calculations. For O2-$LiCoO_2$ and O3-$LiFeO_2$, there are small differences (~0.04) from stoichiometry for oxygen when the oxygen amount was calculated from mass balance. Stoichiometric oxygen was used considering the propagated error for oxygen content from this calculation. For $Li_2Mn_2O_4$, the $LiMnO_2$ formula was used.

3.2. Enthalpy of formation of $LiMO_2$

The enthalpy of formation from oxides (Li_2O and M_2O_3) at 25 °C for $LiMO_2$ (M = Mn, Fe), was calculated from enthalpies of drop solution through thermodynamic cycle (1) in Table 3. The enthalpy of formation from oxides (Li_2O and CoO) plus oxygen at 25 °C for $LiCoO_2$, was calculated using cycle (2) in Table 3. The enthalpies of formation from the elements at 25 °C were determined from the enthalpies of formation from oxides for $LiMO_2$ and the enthalpies of formation from the elements for binary oxides from Ref. [23]. Enthalpies of drop solution (ΔH_{ds}) of binary oxides (Li_2O, Na_2O, Mn_2O_3, Fe_2O_3, and CoO), and $LiMO_2$, and enthalpies of formation (ΔH_f^0) of $LiMO_2$ are listed in Table 4. For β-$LiFeO_2$, enthalpies of drop solution are the same within experimental error for the samples annealed at 400 °C for 16 and 24 days, respectively. This is also the case for γ-$LiFeO_2$ annealed at 475 °C for 12 and 30 days. The data for β-$LiFeO_2$ annealed for 24 days and γ-$LiFeO_2$ annealed for 12 days were used in the calorimetric calculations. The enthalpies of drop solution for *m*-$LiMnO_2$ and $Li_2Mn_2O_4$, after correction for carbonate impurity, would have larger uncertainties if the error in the amount of Li_2CO_3 was considered. An error of 1 wt% in the amount of Li_2CO_3 (which is large in terms of TG analysis) corresponds to ~1.2 kJ/mol in enthalpy of drop solution.

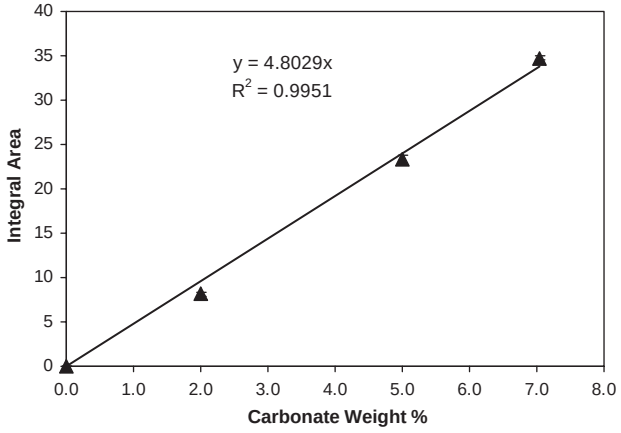

Fig. 2. Integral area of the spectral region 1310–1591 cm^{-1} in the FTIR spectra as a function of Li_2CO_3 concentration (wt%).

There are very few thermodynamic data reported for $LiMO_2$ in the literature. Table 5 compiles the available thermochemical data for $LiMO_2$ (M = Mn, Fe, and Co). The free energy data for $LiCoO_2$ from EMF measurements are not included but are given elsewhere [16]. For α-$LiFeO_2$, the entropy of formation from the elements at 25 °C, $\Delta S_{f,el}^0$, was calculated from standard entropy data (29.09 ± 0.20, 27.09 ± 0.13, 205.15 ± 0.02 J/(mol K) [23], and 75.3 ± 0.8 J/(mol K) [26] for Li, Fe, O_2, and α-$LiFeO_2$, respectively). $\Delta S_{f,el}^0$ (α-$LiFeO_2$) = -186.0 ± 0.8 J/(mol K). Therefore the Gibbs free energy of formation from the elements at 25 °C, $\Delta G_{f,el}^0$ (α-$LiFeO_2$) = -694.3 ± 1.8 kJ/mol, using the $\Delta H_{f,el}^0$ data determined in this study. It agrees very well with the Gibbs free energy of formation from the elements at 27 °C reported by Yokokawa et al. (−694.16 kJ/mol) [27]. Due to the lack of standard entropy data for other compounds, one cannot as readily compare the newly measured enthalpy data with the free energy data in the literature. However, the entropy of formation from oxides (Li_2O and M_2O_3), $\Delta S_{f,ox}^0$, for $LiMO_2$ should be small since no gases are involved. As a first approximation, the entropy of formation from the elements, $\Delta S_{f,el}^0$, can be estimated assuming $\Delta S_{f,ox}^0 = 0$ J/(mol K). Thus $\Delta S_{f,el}^0$ ($LiMO_2$) = 0.5 ($\Delta S_{f,el}^0(Li_2O) + \Delta S_{f,el}^0(M_2O_3)$). The

Table 2
ICP–OES analytical results and compositions of four $LiMO_2$ samples

Compound	ICP results (wt%)			Composition
	Li	Na	*M*	
m-$LiMnO_2$	7.15	0.65	58.25	$Li_{0.972}Na_{0.027}MnO_2$
O2-$LiCoO_2$	6.49	0.53	59.80	$Li_{0.921}Na_{0.023}CoO_2$
O3-$LiFeO_2$	6.81	1.70	58.77	$Li_{0.932}Na_{0.070}FeO_2$
$Li_2Mn_2O_4$	7.96	—	59.54	$Li_2Mn_2O_4$ ($LiMnO_2$)

Table 3
Thermodynamic cycles for the determination of the enthalpy of formation from oxides at 25 °C for $LiMO_2$ (M = Mn, Fe) (cycle 1), and the enthalpy of formation from oxides and oxygen at 25 °C for $LiCoO_2$ (cycle 2)

Reaction	ΔH
Cycle1	
Li_2O (s, 25 °C) → Li_2O (sln, 701 °C)	$\Delta H_1 = \Delta H_{ds}$ (Li_2O)
M_2O_3 (s, 25 °C) → M_2O_3 (sln, 701 °C)	$\Delta H_2 = \Delta H_{ds}$ (M_2O_3)
$LiMO_2$ (s, 25 °C) → 0.5 Li_2O (sln, 701 °C) + 0.5 M_2O_3 (sln, 701 °C)	$\Delta H_3 = \Delta H_{ds}$ ($LiMO_2$)
2Li (s, 25 °C) + 0.5O_2 (g, 25 °C) → Li_2O (s, 25 °C)	$\Delta H_4 = \Delta H^0_{f,el}(Li_2O)$
2M(s, 25 °C) + 1.5 O_2 (g, 25 °C) → M_2O_3 (s, 25 °C)	$\Delta H_5 = \Delta H^0_{f,el}(M_2O_3)$
0.5 Li_2O (s, 25 °C) + 0.5 M_2O_3 (s, 25 °C) → $LiMO_2$ (s, 25 °C)	$\Delta H_6 = \Delta H^0_{f,ox}(LiMO_2)$
$\Delta H_6 = 0.5\ \Delta H_1 + 0.5\ \Delta H_2 - \Delta H_3$	
Li (s, 25 °C) + M(s, 25 °C) + O_2 (g, 25 °C) → $LiMO_2$ (s, 25 °C)	$\Delta H_7 = \Delta H^0_{f,el}(LiMO_2)$
$H_7 = 0.5\ \Delta H_4 + 0.5\ \Delta H_5 + \Delta H_6$	
Cycle2	
Li_2O (s, 25 °C) → Li_2O (sln, 701 °C)	$\Delta H_1 = \Delta H_{ds}$ (Li_2O)
MO (s, 25 °C) → MO (sln, 701 °C)	$\Delta H_8 = \Delta H_{ds}$ (MO)
$LiMO_2$ (s, 25 °C) → 0.5 Li_2O (sln, 701 °C) + MO (sln, 701 °C) + 0.25 O_2 (g, 701 °C)	$\Delta H_9 = \Delta H_{ds}$ ($LiMO_2$)
O_2 (g, 25 °C) → O_2 (g, 701 °C)	$\Delta H_{10} = \int_{298}^{974} C_p(O_2)\,dT$
2 Li (s, 25 °C) + 0.5 O_2 (g, 25 °C) → Li_2O (s, 25 °C)	$\Delta H_4 = \Delta H^0_{f,el}(Li_2O)$
M(s, 25 °C) + 0.5 O_2 (g, 25 °C) → MO (s, 25 °C)	$\Delta H_{11} = \Delta H^0_{f,el}(MO)$
0.5 Li_2O (s, 25 °C) + MO (s, 25 °C) + 0.25 O_2 (g, 25 °C) → $LiMO_2$ (s, 25 °C)	$\Delta H_{12} = \Delta H^0_{f,ox/O_2}(LiMO_2)$
$\Delta H_{12} = 0.5\ \Delta H_1 + \Delta H_8 + 0.25\Delta H_{10} - \Delta H_9$	
Li (s, 25 °C) + M(s, 25 °C) + O_2 (g, 25 °C) → $LiMO_2$ (s, 25 °C)	$\Delta H_{13} = \Delta H^0_{f,el}(LiMO_2)$
$\Delta H_{13} = 0.5\ \Delta H_4 + \Delta H_{11} + \Delta H_{12}$	

s = solid, g = gas, sln = in solution.
$\Delta H^0_{f,el}$ for Li_2O, Mn_2O_3, Fe_2O_3, and CoO, and C_p (O_2) are from Ref. [23].

estimated free energy of formation from the elements for o-$LiMnO_2$ is listed in Table 5. The estimated $\Delta G^0_{f,el}$ agrees reasonably well with that reported by Yokokawa et al. [27].

The enthalpy of formation from oxides at 25 °C indicates the relative stability of the polymorphs of $LiMO_2$. The differences in enthalpy between the polymorphs are relatively small. Therefore the entropy term must be considered. For $LiFeO_2$, ΔS ($\gamma \rightarrow \alpha$) = 9.9 ± 0.9 J/(mol K) at 660 °C (see Section 3.3). Then $\Delta S^0_{f,el}(\gamma\text{-}LiFeO_2) = -195.9 \pm 1.2$ J/(mol K) using $\Delta S^0_{f,el}(\alpha\text{-}LiFeO_2) = -186.0 \pm 0.8$ J/(mol K) and assuming ΔS ($\gamma \rightarrow \alpha$) = 9.9 ± 0.9 J/(mol K) at 25 °C. Thus the estimated Gibbs free energy of formation from the elements for γ-$LiFeO_2$ is −700.6 ± 1.9 kJ/mol, slightly more exothermic than that of α-$LiFeO_2$. Therefore at room temperature the ordered γ phase is more stable in terms of both enthalpy and Gibbs free energy, but lower in entropy than the disordered α phase. Due to the lack of entropy data, this calculation cannot be done for other compounds.

Fig. 3 shows the relative stability of the polymorphs of $LiMO_2$ (M = Mn, Fe, and Co) with enthalpies relative to the lowest enthalpy form. For $LiFeO_2$, the γ phase is the lowest enthalpy form and the α-$NaFeO_2$ structured $LiFeO_2$ has the highest enthalpy. For α-, β-, and γ-$LiFeO_2$, the β phase is intermediate in enthalpy. Orthorhombic $LiMnO_2$ (o-$LiMnO_2$) is slightly more stable in enthalpy than tetragonal $LiMnO_2$ ($Li_2Mn_2O_4$) which in turn is more stable than monoclinic layered $LiMnO_2$ (m-$LiMnO_2$). The relative energetic stability of m-$LiMnO_2$ and o-$LiMnO_2$ determined experimentally agrees with that predicted by first principles calculations [10,32]. The factors that influence the structural stability of $LiMnO_2$ include Jahn–Teller distortion and magnetism [10,32]. The new polymorph O2-$LiCoO_2$ is less stable in enthalpy than O3-$LiCoO_2$. This is expected from crystal chemistry because in O3-$LiCoO_2$, the LiO_6 and CoO_6 octahedra share only edges while in O2-$LiCoO_2$, they share both edges and faces.

3.3. Phase transformations in $LiFeO_2$

The phase transformations in $LiFeO_2$ were studied by DSC. Fig. 4 and 5 show the DSC traces for heating/cooling rates of 5 and 10 °C/min, respectively. The temperatures of the phase transitions observed using DSC are listed in Table 6. The ordering of α to β or to γ is very sluggish. No appreciable phase transition was

Table 4
Enthalpy of drop solution in sodium molybdate at 701 °C, ΔH_{ds}, enthalpy of formation from oxides (or from oxides and oxygen) at 25 °C, $\Delta H^0_{f,ox}$, and enthalpy of formation from the elements $\Delta H^0_{f,el}$, of LiMO_2

Compound	ΔH_{ds} (kJ/mol)[a]	$\Delta H^0_{f,ox}$ (kJ/mol)	$\Delta H^0_{f,el}$ (kJ/mol)
α-$LiFeO_2$	39.04±0.57 (10)	−37.74±1.28	−749.8±1.8
β-$LiFeO_2$	43.92±0.43 (9)[b]	−42.62±1.23	−754.7±1.7
	43.94±0.35 (2)[c]		
γ-$LiFeO_2$	48.25±0.68 (13)[d]	−46.95±1.34	−759.0±1.8
	47.10±0.95 (6)[e]		
O3-$LiFeO_2$[f]	0.3461±0.0075 (14) kJ/g[g]	−34.31±1.30	−740.0±1.8
	31.25±0.73[h]		
o-$LiMnO_2$	97.52±1.00 (12)	−61.08±1.60	−839.5±2.0
m-$LiMnO_2$[f]	1.0073±0.0090 (9) kJ/g[g]	−52.98±1.51	−828.7±1.9
	87.79±0.90[h]		
$Li_2Mn_2O_4$	1.0562±0.0095 (14) kJ/g[g]	−116.21±3.11	−1673.1±3.9
	189.11±1.86[h]		
t-$LiMnO_2$	94.55±0.93[h]	−58.10±1.55	−836.6±1.9
O3-$LiCoO_2$	116.82±1.17 (10) [i]	−142.54±1.69	−679.4±2.4
O2-$LiCoO_2$[f]	110.12±1.39 (12)	−134.31±1.79	−652.3±2.4
Li_2CO_3	162.76±0.77 (8)[i]		
Li_2O	−93.02±2.24[i]		
CoO	15.35±0.45 (7)[i]		
Mn_2O_3	165.92±1.08 (10)		
Fe_2O_3	95.63±0.50 (27)[j]		
Na_2O	−217.56±4.25[k]		

[a]Uncertainties are two standard deviations of the mean, numbers in () are the numbers of experiments.
[b]Sample annealed at 400 °C for 24 days.
[c]Sample annealed at 400 °C for 16 days.
[d]Sample annealed at 475 °C for 12 days.
[e]Sample annealed at 475 °C for 30 days.
[f]For O3-$LiFeO_2$, *m*-$LiMnO_2$ and O2-$LiCoO_2$, calculations of formation enthalpy consider the real composition including sodium in the cycle.
[g]Enthalpy of drop solution before correction for surface water or carbonate. The data are in kJ/g as indicated in the table because the sample contains a second minor phase.
[h]Enthalpy of drop solution after correction for surface water or carbonate. *t*-$LiMnO_2$ uses the formula of LiMO_2 calculated from $Li_2Mn_2O_4$, for comparison with other compounds. The data are in kJ/mol as for all other enthalpies of drop solution for pure compounds.
[i]Ref. [16].
[j]Ref. [24].
[k]Ref. [25].

detected by DSC when heating/cooling the α phase. In contrast, the disorder transition $\gamma \rightarrow \alpha$ occurs more readily as evidenced by an endothermic peak during heating of γ-$LiFeO_2$ at ~693 °C (10 °C/min) or ~690 °C (5 °C/min), which agrees with the observations of Kato [33]. β-$LiFeO_2$ exhibits two endothermic peaks during heating, namely, 630 and 688 °C at 5 °C/min, or 588 and 688 °C at 10 °C/min, ascribed to the transitions of the β phase to an unknown intermediate phase (denoted "*x*" phase) and this "*x*" phase to the α phase. The exothermic peak corresponding to the ordering of α to γ during cooling was not detected even with a cooling rate of 1 °C/min, which confirms the sluggishness of the transformation on cooling. However, there is another ordering transition occurring during cooling at ~436 °C with a broad exothermic peak. This transition is believed to be $\alpha \rightarrow \beta$, as confirmed by the XRD patterns of the samples (β and γ-$LiFeO_2$) after DSC (mixture of α and β phases). The disordered α phase obtained from heating the β or γ phase in the DSC experiments underwent some degree of ordering when cooling and the amount of the ordered phase (β) is related to the cooling rate. The products after DSC cooling runs of β and γ-$LiFeO_2$ are a mixture of two phases (α and β) with the α phase as the major phase. For the samples undergoing DSC at 10 °C/min, the α phase is predominant in the cooled products. The products after DSC at 5 °C/min contain a larger amount of β phase than those cooled at 10 °C/min. For α-$LiFeO_2$ after DSC, only the α phase was detected by XRD. Phase transitions detectable by DSC in β- and γ-$LiFeO_2$ suggest that the disordered α phase obtained after heating in the DSC experiment has some degrees of short range order, which facilitates the ordering ($\alpha \rightarrow \beta$) during cooling. Alternately, it may contain some remnants of the ordered phase as nuclei for further ordering.

Table 5
Thermochemical data for LiMO_2 (M = Fe, Mn, and Co)

Compound	Thermochemical data (kJ/mol)	T (°C)	Method and references
α-$LiFeO_2$	$\Delta H^0_{f,el} = -749.8 \pm 1.8$	25	Drop solution calorimetry, this study
	$\Delta G^0_{f,el} = -694.3 \pm 1.8$	25	Calculated from $\Delta H^0_{f,el}$ this study and S^0 data from [23,26]
	$\Delta G^0_{f,el} = -645.09$	400	Electrochemical [28]
	$\Delta G^0_{f,el} = -694.16$	27	[27]
	$\Delta G^0_{f,el} = (-752 \pm 1) + (0.187 \pm 0.003)$ (T/K)	400–600	EMF [29]
	$S^0 = 75.3 \pm 0.8$ J/(mol K)	25	[26]
o-$LiMnO_2$	$\Delta H^0_{f,el} = -839.5 \pm 2.0$	25	Drop solution calorimetry, this study
	$\Delta G^0_{f,el} = -782.7 \pm 2.0$	25	Estimated from $\Delta S^0_{f,el} = -190.6$ J/(mol K)[a] and $\Delta H^0_{f,el}$ determined this study
	$\Delta G^0_{f,el} = -745.63$	400	Electrochemical [28]
	$\Delta G^0_{f,el} = -792.85$	27	[27]
	$\Delta G^0_{f,el} = -947 \pm 13$	407	EMF [30]
	$\Delta G^0_{f,el} = -949 \pm 13$	467	EMF [30]
	$\Delta G^0_{f,el} = -950 \pm 13$	527	EMF [30]
O3-$LiCoO_2$	$\Delta H^0_{f,el} = -679.4 \pm 2.4$	25	Drop solution calorimetry[b] [16]
	$\Delta G^0_{f,el} = -616.2 \pm 2.4$	25	Calculated from $\Delta H^0_{f,el}$ this study and S^0 data from [23,31]
	$\Delta G^0_{f,el} = -619.65$	27	[27]
	$S^0 = 52.45$ J/(mol K)	25	[31]

[a] $\Delta S^0_{f,el}$ was estimated using standard entropy data from [23], see text.
[b] Enthalpy of formation determined from calorimetry in sodium molybdate.

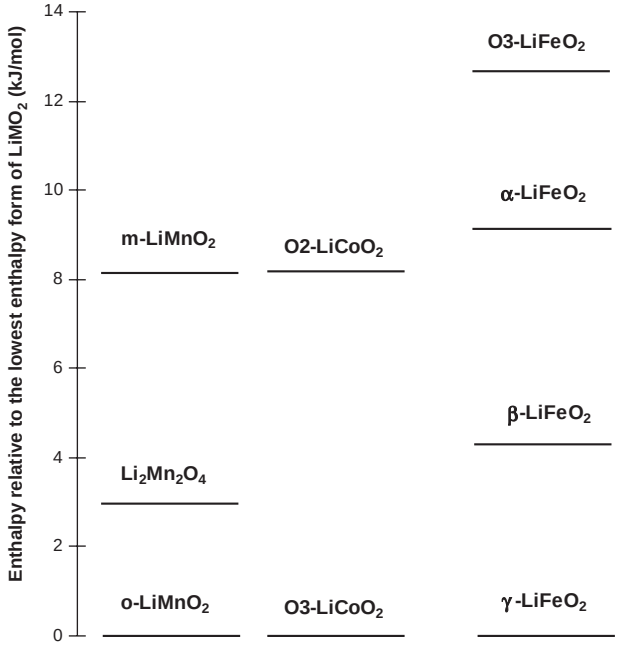

Fig. 3. Enthalpy relative to the lowest enthalpy form of LiMO_2 (M = Mn, Fe and Co) showing relative stability of the polymorphs.

In contrast, for the completely disordered as prepared α phase, the ordering transition was restricted by the slow kinetics.

The order–disorder transition between γ and α is thermodynamically reversible with an endothermic heat effect for the disordering transition during heating. Though the ordering on cooling was not detected by DSC, this reflects the kinetic sluggishness of the transition and γ-$LiFeO_2$ is formed from long annealing of α-$LiFeO_2$.

The transition enthalpy at 25 °C was determined from the enthalpy of drop solution of α-, β- and γ-$LiFeO_2$ using the cycle in Table 7. ΔH_{tr} ($\beta \rightarrow \alpha$) is 4.9 ± 0.7 kJ/mol, ΔH_{tr} ($\gamma \rightarrow \beta$) is 4.3 ± 0.8 kJ/mol and ΔH_{tr} ($\gamma \rightarrow \alpha$) is 9.2 ± 0.9 kJ/mol. This indicates that at room temperature, γ is the stable phase while α, β are metastable. A rough estimation of the transition entropy for $\gamma \rightarrow \alpha$ at the transition temperature, is 9.6 ± 0.9 J/(mol K) at 690 °C (determined from DSC at 5 °C/min), or 9.9 ± 0.9 J/(mol K) at 660 °C (determined by dilatometry by Kato [33]), assuming the transition enthalpy at the transition temperature is the same as that at 25 °C. The maximum change in configurational entropy for γ- to α-$LiFeO_2$ is 2Rln2 ($= 11.5$) J/(mol K), slightly larger than ΔS_{tr} estimated from the experimental transition enthalpy. This suggests that either there is some short-range order in the as prepared α phase or the γ phase is not completely ordered.

The β phase is intermediate in enthalpy between γ and α. It may have a stability field at intermediate temperatures or it may be metastable, depending largely

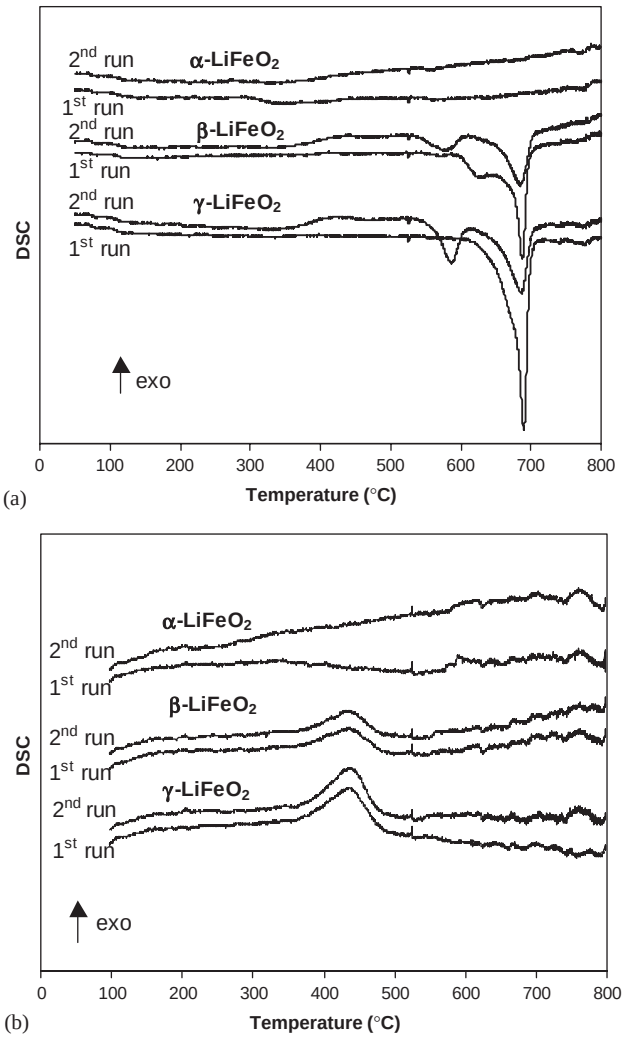

Fig. 4. DSC traces of $LiFeO_2$ at a heating/cooling rate of 5 °C/min: (a) heating and (b) cooling. In the 2nd runs, the phases are $\alpha+\beta$ for samples after the 1st runs of β- and γ-$LiFeO_2$, and α phase in the case of α-$LiFeO_2$.

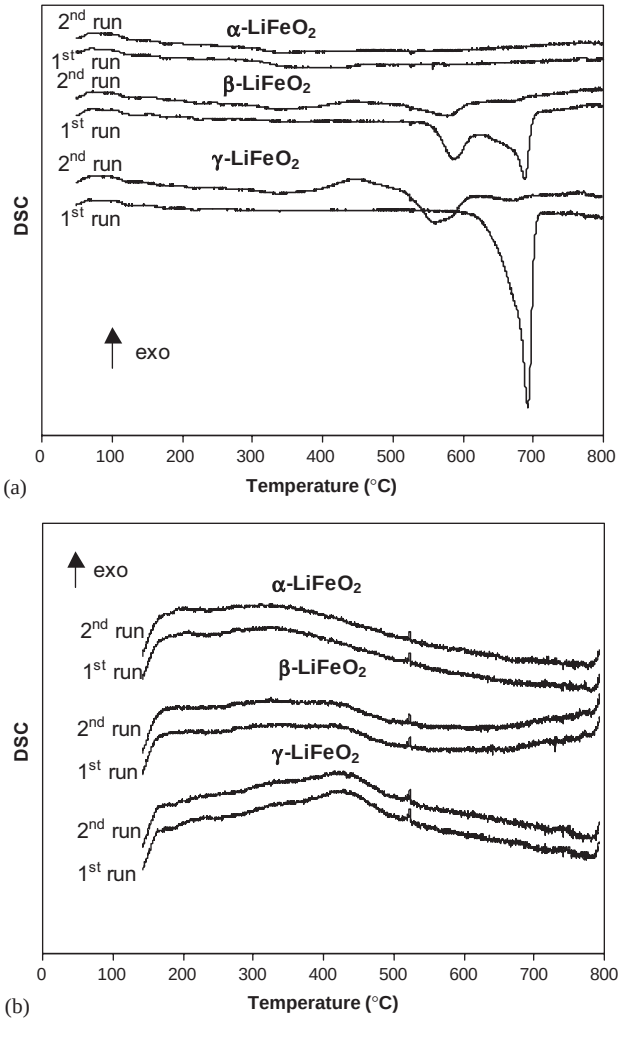

Fig. 5. DSC traces of $LiFeO_2$ at a heating/cooling rate of 10 °C/min: (a) heating and (b) cooling. In the 2nd runs, the phases are $\alpha+\beta$ for samples after the 1st runs of β- and γ-$LiFeO_2$, and α phase in the case of α-$LiFeO_2$.

on the (presently unknown) entropy of transition. The pattern of transformations involving β seen in DSC is probably controlled by kinetics as well as thermodynamics and does not provide definitive evidence on the stability or metastability of the β phase.

4. Conclusions

Polymorphs of $LiMO_2$ (M = Mn, Fe, and Co) were synthesized successfully by soft chemistry and solid-state reaction methods. The relative stability of the different structures of the compound $LiMO_2$ was studied by determining their enthalpies of formation from oxides (Li_2O and M_2O_3, M = Mn, Fe), or from oxides (Li_2O and CoO) plus oxygen at 25 °C using high-temperature oxide melt solution calorimetry. The enthalpy differences between the different structures of $LiMO_2$ are relatively small. Orthorhombic $LiMnO_2$, γ-$LiFeO_2$, and α-$NaFeO_2$ structured (O3) $LiCoO_2$ are the form with lowest enthalpy among the polymorphs of $LiMnO_2$, $LiFeO_2$ and $LiCoO_2$, respectively.

Phase transformations in $LiFeO_2$ were investigated by differential scanning calorimetry and high-temperature oxide melt solution calorimetry. The ordering transition is very sluggish whereas disorder occurs more readily. The ordering enthalpy for α to γ is -9.2 ± 0.9 kJ/mol at 25 °C. The phase transition enthalpies at 25 °C for transformations $\beta \rightarrow \alpha$, $\gamma \rightarrow \beta$, and $\gamma \rightarrow \alpha$ are 4.9 ± 0.7, 4.3 ± 0.8 and 9.2 ± 0.9 kJ/mol, respectively. The γ phase is the stable form of $LiFeO_2$ at room temperature and the α phase is the stable form at high temperature. The β phase may have a stability field at intermediate temperatures.

Table 6
Temperatures (in °C) of phase transitions on heating ($\uparrow T_{tr}$) and cooling ($\downarrow T_{tr}$) for $LiFeO_2$

Compound	1st run			2nd run		
	$\uparrow T_{tr1}$	$\uparrow T_{tr2}$	$\downarrow T_{tr}$	$\uparrow T_{tr1}$	$\uparrow T_{tr2}$	$\downarrow T_{tr}$
5 °C/min heating/cooling, 30–800 °C						
γ-$LiFeO_2$	689.5	—	436.3	586.6	686.3	439.9
β-$LiFeO_2$	629.7	687.7	437.3	577.6	683.9	435.9
α-$LiFeO_2$	No peaks observed					
10 °C/min heating/cooling, 30–800 °C						
γ-$LiFeO_2$	692.6	—	419.1[a]	561.6	671[b]	411.9[a]
β-$LiFeO_2$	588.2	687.8	[c]	577.3	672[b]	[c]
α-$LiFeO_2$	No peaks observed					

[a]Very weak diffuse peak.
[b]Very weak peak.
[c]No appreciable peak, weaker than that in γ-$LiFeO_2$ [a]

Table 7
Thermodynamic cycle for the determination of transition enthalpy at 25 °C in $LiFeO_2$

Reaction	ΔH
α-$LiFeO_2$ (s, 25 °C) → 0.5 Li_2O (sln, 701 °C) + 0.5 Fe_2O_3 (sln, 701 °C)	$\Delta H_{14} = \Delta H_{ds}$ (α-$LiFeO_2$)
β-$LiFeO_2$ (s, 25 °C) → 0.5 Li_2O (sln, 701 °C) + 0.5 Fe_2O_3 (sln, 701 °C)	$\Delta H_{15} = \Delta H_{ds}$ (β-$LiFeO_2$)
γ-$LiFeO_2$ (s, 25 °C) → 0.5 Li_2O (sln, 701 °C) + 0.5 Fe_2O_3 (sln, 701 °C)	$\Delta H_{16} = \Delta H_{ds}$ (γ-$LiFeO_2$)
β-$LiFeO_2$ (s, 25 °C) → α-$LiFeO_2$ (s, 25 °C)	$\Delta H_{17} = \Delta H_{tr}$ ($\beta \rightarrow \alpha$)
γ-$LiFeO_2$ (s, 25 °C) → β-$LiFeO_2$ (s, 25 °C)	$\Delta H_{18} = \Delta H_{tr}$ ($\gamma \rightarrow \beta$)
γ-$LiFeO_2$ (s, 25 °C) → α-$LiFeO_2$ (s, 25 °C)	$\Delta H_{19} = \Delta H_{tr}$ ($\gamma \rightarrow \alpha$)
$\Delta H_{17} = \Delta H_{15} - \Delta H_{14}$	
$\Delta H_{18} = \Delta H_{16} - \Delta H_{15}$	
$\Delta H_{19} = \Delta H_{16} - \Delta H_{14}$	

Acknowledgments

We thank Y. Moriya for valuable discussions. This work was supported by the US Department of Energy (Grant DE-FG0397SF 14749).

References

[1] T.A. Hewston, B.L. Chamberland, J. Phys. Chem. Solids 48 (1987) 97.
[2] D.G. Kellerman, Russ. Chem. Rev. 70 (2001) 777.
[3] M. Tabuchi, S. Tsutsui, C. Masquelier, R. Kanno, K. Ado, I. Matsubara, S. Nasu, H. Kageyama, J. Solid State Chem. 140 (1998) 159.
[4] A.R. Armstrong, P.G. Bruce, Nature 381 (1996) 499.
[5] G. Vitins, K. West, J. Electrochem. Soc. 144 (1997) 2587.
[6] T. Shirane, R. Kanno, Y. Kawamoto, Y. Takeda, M. Takano, T. Kamiyama, F. Izumi, Solid State Ion. 79 (1995) 227.
[7] R. Kanno, T. Shirane, Y. Kawamoto, Y. Takeda, M. Takano, M. Ohashi, Y. Yamaguchi, J. Electrochem. Soc. 143 (1996) 2435.
[8] C. Delmas, C. Fouassier, P. Hagenmuller, Physica B 99 (1980) 81.
[9] E.J. Wu, P.D. Tepesch, G. Ceder, Philos. Mag. B 77 (1998) 1039.
[10] S.K. Mishra, G. Ceder, Phys. Rev. B 59 (1999) 6120.
[11] J.C. Anderson, M. Schieber, J. Phys. Chem. Solids 25 (1964) 961.
[12] J.C. Anderson, M. Schieber, Sci. Ceram. 2 (1965) 345.
[13] R. Famery, P. Bassoul, F. Queyroux, J. Solid State Chem. 57 (1985) 178.
[14] D. Carlier, I. Saadoune, L. Croguennec, M. Menetrier, E. Suard, C. Delmas, Solid State Ion. 144 (2001) 263.
[15] J.B. Tarascon, D. Guyomard, J. Electrochem. Soc. 138 (1991) 2864.
[16] M. Wang, A. Navrotsky, Solid State Ion. 166 (2004) 167.
[17] C. Laberty, A. Navrotsky, Geochim. Cosmochim. Acta 62 (1998) 2905.
[18] J. Majzlan, A. Navrotsky, B. Evans, Phys. Chem. Miner. 29 (2002) 515.
[19] A. Navrotsky, Phys. Chem. Miner. 2 (1977) 89.
[20] A. Navrotsky, Phys. Chem. Miner. 24 (1997) 222.
[21] A. Navrotsky, O.J. Kleppa, J. Inorg. Nucl. Chem. 30 (1968) 479.
[22] M. Wang and A. Navrotsky, J. Solid State Chem. (2004), in press.
[23] R.A. Robie, B.S. Hemingway, Thermodynamic properties of minerals and related substances at 298.15 K and 1 bar (10^5 Pa) pressure and at higher temperatures, US Geological Survey Bulletin, No. 2131, Washington, DC, 1995.
[24] J. Majzlan, A. Navrotsky, J. Neil, Geochim. Cosmochim. Acta 66 (2002) 1839.
[25] F. Tessier, A. Navrotsky, A. Le Sauze, R. Marchand, Chem. Mater. 12 (2000) 148.

[26] E.G. King, J. Am. Chem. Soc. 77 (1955) 3189.
[27] H. Yokokawa, N. Sakai, K. Yamaji, T. Horita, M. Ishikawa, Solid State Ion. 113-115 (1998) 1.
[28] N.A. Godshall, I.D. Raistrick, R.A. Huggins, J. Electrochem. Soc. 131 (1984) 543.
[29] K. Kawamura, K. Asano, S. Nagano, A. Kaimai, K. Yashiro, Y. Nigara, T. Kawada, J. Mizusaki, Ionic and mixed conducting ceramics IV, in: T.A. Ramanarayanan (Ed.), Proceedings of the Fourth International Symposium, The Electrochemical Society, Inc., Pennington, NJ, 2002, p. 272.
[30] G. Rog, W. Kucza, A. Kozlowska-Rog, J. Chem. Thermodyn. 36 (2004) 473.
[31] H. Kawaji, M. Takematsu, T. Tojo, T. Atake, A. Hirano, R. Kanno, J. Therm. Anal. Calorim. 68 (2002) 833.
[32] G. Ceder, S.K. Mishra, Electrochem. Solid-State Lett. 2 (1999) 550.
[33] E. Kato, Bull. Chem. Soc. Jpn. 31 (1958) 108.